ISSN 0957-4484

NANOTECHNOLOGY

VOLUME 19 NUMBER 40 8 OCTOBER 2008

www.iop.org/journals/nano

Featured article

Fabrication of large arrays of high-aspect-ratio single-crystal silicon columns with isolated vertically aligned multi-walled carbon nanotube tips

L F Velásquez-García and A I Akinwande

IOP Publishing

Nanotechnology **19** (2008) 405305 (6pp) doi:10.1088/0957-4484/19/40/405305

Fabrication of large arrays of high-aspect-ratio single-crystal silicon columns with isolated vertically aligned multi-walled carbon nanotube tips

L F Velásquez-García[1] **and A I Akinwande**[2]

[1] Microsystems Technology Laboratories, Massachusetts Institute of Technology, 77 Massachusetts Avenue, Office 39-657, Cambridge, MA 02139, USA
[2] Department of Electrical Engineering and Computer Science, Massachusetts Institute of Technology, Cambridge, MA 02139, USA

E-mail: Velasquez@ alum.mit.edu

Received 29 April 2008, in final form 3 July 2008
Published 26 August 2008
Online at stacks.iop.org/Nano/19/405305

Abstract
This paper describes the fabrication of large arrays (10^6 units in 1 cm^2) of 100 μm tall, single-crystal silicon columns with submicron tip cross-sections. The columns are formed using thin film deposition and growth, reactive ion etching, and deep reactive ion etching. The columns can be either slightly tapered or have pencil-like morphology with nanoscaled tip diameter (41 nm). Conformal thin film coating was used to substantially and uniformly modify the porous structure and, thus, vary by orders of magnitude the fluid permeability of the structure. Gaps between the vertical pillars were varied between 9 μm and 50 nm. Isolated 45 nm diameter, 5 μm tall plasma enhanced chemical vapour deposited multi-walled carbon nanotubes (MWNTs) were grown on the top surface of the columns using a 7 nm thick evaporated Ni film as catalyst. Field emission characterization of the resulting structure was conducted and it is in agreement with scanning electron micrographs of the MWNTs.

1. Introduction

Several techniques have been developed for the fabrication of high-aspect-ratio structures, including x-ray LIGA [1, 2], SU-8 [3, 4], focused ion-beam etching [5, 6], glancing-angle deposition (GLAD) [7, 8], electrochemical etching [9, 10], and deep reactive ion etching (DRIE) [11–13]. High-aspect-ratio microstructures have been used to enable efficient operation of a number of microelectromechanical systems (MEMS) such as photonic band gap (PBG) devices [14], chemical reactors [15, 16], micro-engines [17, 18], and sensors [19, 20]. In this work we used a high-selectivity DRIE process to fabricate a monolithic, dense array of high-aspect-ratio single-crystal silicon columns distributed in a particular spatial fashion with low column-to-column variation. The columns could be either slightly tapered or have pencil-like morphology and nanoscaled tip diameter. We were also able to grow isolated plasma enhanced chemical vapour deposited (PECVD) MWNTs [21] on top of the column arrays without the need of electron beam lithography [22]. We used low-pressure chemical vapour deposited (LPCVD), physical vapour deposited (PVD), thermally grown, and PECVD films [23] to fabricate the silicon columns and the MWNT catalyst pads, and to vary the porosity of the column array over a wide range while achieving uniform nanoscaled porous structures.

There are several applications that would benefit from using the structure that we report. First, the monolithic, dense, high-aspect-ratio tapered column arrays could be used as invasive probes for tissue studies, in particular in neurological and ophthalmologic investigations [24–26]. Second, the array of columns can be used as a custom-designed porous material with low morphological variation for flow control, i.e., as hydraulic impedance, monolithically formed with the rest of the MEMS [27]. In this case, nanofluidic applications such as micro-total analysis systems (μTAS) [28, 29], nanoelectromechanical system (NEMS)

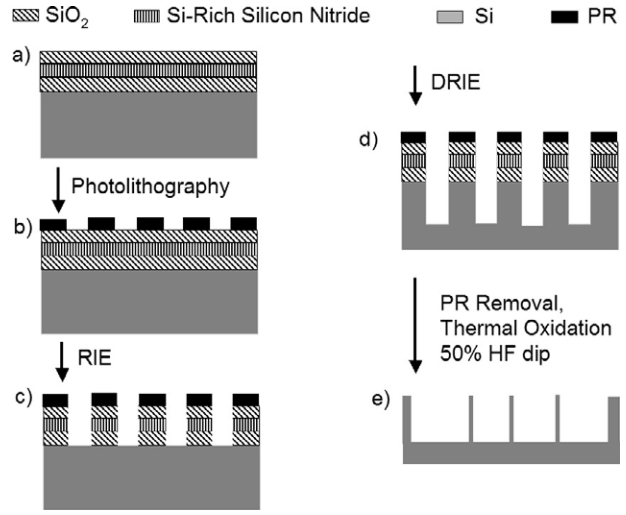

Figure 1. High-aspect-ratio silicon column array process flow schematic.

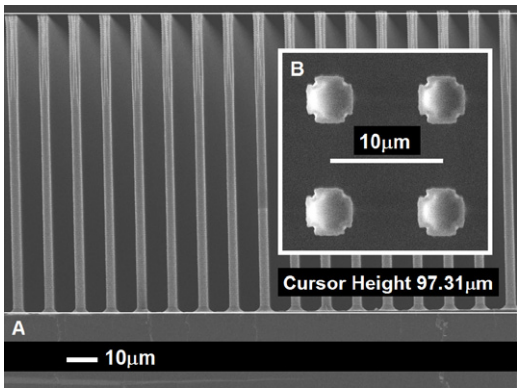

Figure 2. Side view (A) and top view (B) of a silicon column array after DRIE. The corners of the columns have notches 750 nm wide from PR overdevelopment.

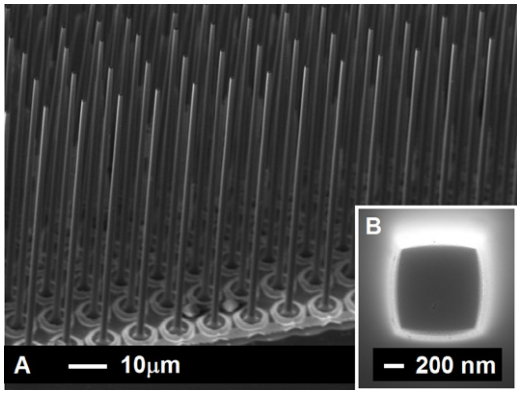

Figure 3. Field view of a high-aspect-ratio silicon column array with submicron tip cross-section (A), and tip cross-section detail (B).

liquid chromatographers [30] and gas chromatographers [31] could be implemented. Third, the structure can also be used to make uniform and reliable MWNT-based field emission electron sources [32, 33]. For this application, the Si columns act as ungated field effect transistors (FETs) that effectively limit the current through each emitter, taking advantage of the velocity saturation of electrons in the semiconductor lattice [34]. Also, the vertical nature and small footprint of the ballasting element allows substantially denser field emitter arrays.

2. Fabrication

2.1. Fabrication of tapered/pencil-like high-aspect-ratio silicon columns

Figure 1 outlines the procedure to fabricate monolithic dense arrays of high-aspect-ratio, tapered, silicon columns with submicron cross-section.

The fabrication of the structure starts with a blank ⟨100⟩ single-crystal silicon substrate. Then, a 500 nm thick silicon dioxide layer is thermally grown, followed by the deposition of a 500 nm thick LPCVD silicon-rich silicon nitride film and a 500 nm thick PECVD silicon dioxide film (figure 1(a)). The top silicon dioxide film is used as a hard mask for etching. The silicon-rich silicon nitride film acts as a diffusion barrier for oxygen in a later thermal oxidation step. The lower silicon dioxide layer prevents the formation of the collateral 'bird's beak' due to 2D oxidation of silicon [35]. Contact lithography is next used to transfer the column array pattern to a previously spun-coated 2 μm thick OCG 824 thin positive photoresist (PR) film (figure 1(b)). The column pattern is composed of an array of 6 μm $\times$ 6 μm squares with 10 μm column pitch. The film is overexposed to thin out the corners of the squares to facilitate the tapering of the columns in later process steps. After photolithography is completed, reactive ion etching (RIE) of the thin film stack is conducted (figure 1(c)). After the film stack is etched, 100 μm tall high-aspect-ratio columns are patterned into the silicon substrate using DRIE (figure 1(d)). The substrate is then cleaned and wet oxidized at 1050 °C to grow a 2 μm thick silicon dioxide film. We use a 50% HF etch to remove the oxide and the hard mask instead of HF vapours because we experimentally observed that the resulting columns are structurally strong enough to withstand wet processing without any particular precaution.

Figure 2 shows the side view and top view of a 100 μm tall silicon column array right after the completion of the DRIE process step. The column array has a 10 μm pitch in either direction. The upper part of the columns has striations because of the overdevelopment of the PR film. The striations extend down about one third of the column's height. At this stage, the columns are about 4.2 μm wide at the top. The roots of the columns are chamfered, making them ideal to withstand mechanical loads. The column chamfering results from the particular DRIE recipe used. Figure 3 shows a field view and tip cross-section detail of a monolithic array of silicon columns after the thermal oxidation and HF etch. The average column tip width of the resulting silicon structure is about 750 nm. The columns are slightly tapered as a result of the oxidation of the striations present at the top of the columns. The presence of taper suggests that the structure could be used for invasive probing applications. The results in figure 3

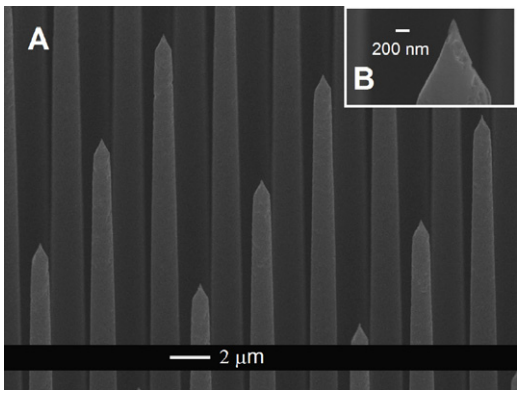

Figure 4. Field view of an array of high-aspect-ratio pencil-like silicon columns with nanosharpened tips (A), and zoomed detail of a tip (B).

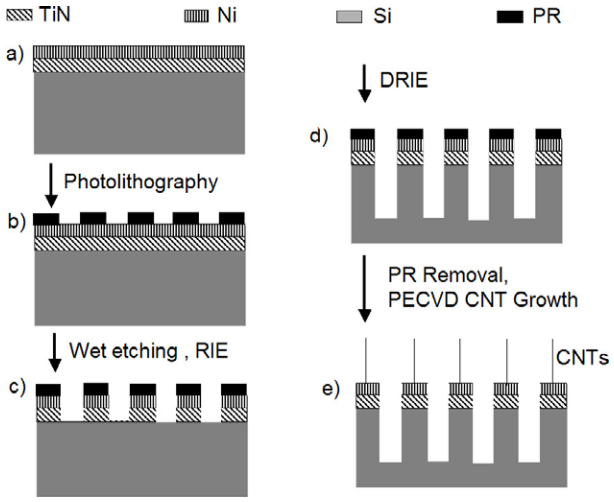

Figure 5. Schematic of modified process flow to fabricate arrays of isolated PECVD MWNTs on top of high-aspect-ratio, single-crystal silicon columns.

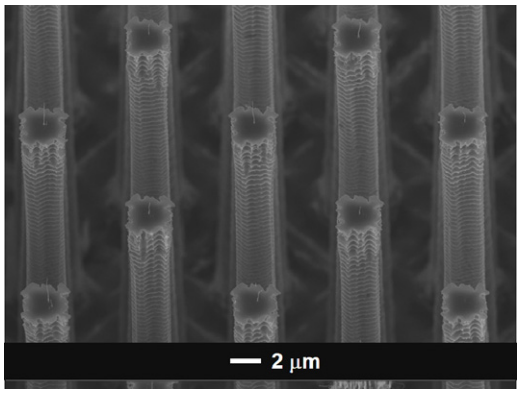

Figure 6. An array of isolated PECVD MWNTs on top of high-aspect-ratio silicon columns.

represent an improvement in the capabilities of DRIE reported in the literature. DRIE aspect-ratio is limited to about 20:1, especially with good etch uniformity and no microloading effects [36, 37]. However, by using a combination of DRIE and oxidation, we were able to obtain large arrays of structures with substantially higher aspect-ratio, while still having excellent etch uniformity. Some researchers have also reported DRIE-patterned needle-like structures. In particular, Hanein *et al* reported needles 230 μm long with an aspect-ratio of 18.4:1, spaced 400 μm [38]. We calculated the aspect-ratio of the needles using as characteristic length the diameter of the body of the silicon needle, measured on the SEMs that they provide in the reference. In contrast, this work reports silicon columns that are 100 μm long with an aspect-ratio of 100:1, and they are spaced 10 μm. Therefore, our arrays of needle-like structures are about 1600 times denser. As a matter of fact, we have created arrays as large as 10^6 pillars in 1 cm^2. Furthermore, if the process flow shown in figure 1 is slightly modified by including a shallow isotropic etch of the silicon right before the DRIE step, large arrays of uniform, pencil-like columns with submicron body cross-section and with tip diameters as small as 41 nm (figure 4) are obtained-contrasted to the 200 nm tip diameter quoted by Hanein *et al*. If we calculated the aspect-ratio of the needles using as characteristic length the tip diameter, then this work represents more than a two-fold improvement with respect to the work reported by Hanein *et al*.

2.2. Growth of isolated PECVD CNTs on top of high-aspect-ratio silicon columns

We explored several techniques to grow isolated PECVD MWNTs on top of the high-aspect-ratio silicon columns. The process flow that resulted in the highest yield and the tallest isolated MWNTs is shown in figure 5. A blank silicon substrate is coated with 7 nm of evaporated Ni on top of a 100 nm thick sputtered TiN film (figure 5(a)). The substrate is then spun-coated with 1 μm thick OCG 824 positive resist, and contact photolithography is used to define the column pattern in the PR (figure 5(b)). The Ni film is etched with the commercial mix TFB from the company Transene (Danvers, MA), and the TiN film is patterned with a chlorine-based RIE step (figure 5(c)). After patterning the thin film stack, the exposed silicon substrate is etched with a DRIE step. At some point during the DRIE the PR film is completely eroded; however, the excellent selectivity of the Ni film with respect to SF_6 plasma chemistries makes it act as etching mask and etch stop of the DRIE step without jeopardizing the remaining part of the processing (figure 5(d)). The substrate is then cleaned with oxygen plasma and put into a PECVD reactor. The process uses a 4:1 mix of ammonia and acetylene to grow MWNTs at 825 °C and 5 Torr [21]. By controlling the Ni wet etch time it is possible to leave a Ni catalyst pad small enough to result in the growth of a single MWNT per column (figure 5(e)).

Figure 6 is a field view of an array of isolated MWNTs on top of the DRIE-patterned silicon columns, tilted 25° with respect to the vertical direction. Figure 7 details a single unit of the PECVD MWNT/silicon column array, tilted 40° with respect to the vertical direction. The typical MWNT diameter was found equal to 45 nm (figure 7(B)). When growing the MWNTs, the height was limited to less than half the distance between two adjacent columns (10 μm) to avoid field shadowing of the MWNTs and thus, facilitate the field

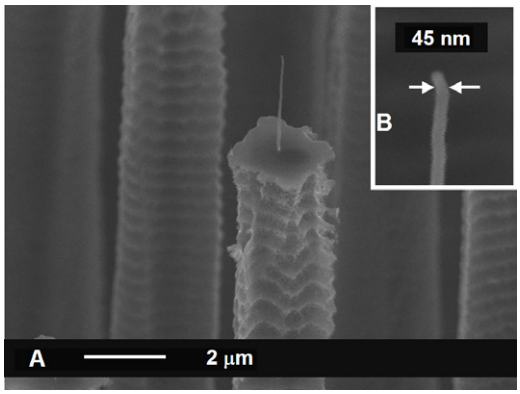

Figure 7. An isolated PECVD MWNT on top of a high-aspect-ratio single-crystal silicon column (A), and metrology of MWNT tip (B).

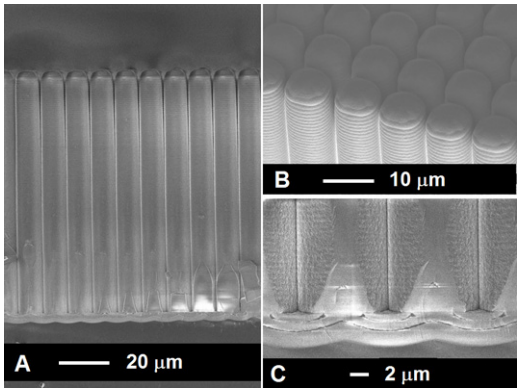

Figure 8. Side view (A), top view (B), and gap-between-adjacent-columns detail (C) of an array of silicon columns that has received a series of silicon dioxide conformal coatings.

emission tests conducted to corroborate their metrology (see section 4) [39].

3. Uniform variation of porous structure

The porosity, i.e., fraction of void space, of a given column array could be varied using conformal coatings. For example, if the 50% HF etch is skipped in the process flow shown in figure 1, it is possible to reduce the gap between adjacent columns with a series of LPCVD poly-crystalline silicon coatings followed by oxidation, effectively decreasing the porosity (figure 8). In figure 3, the average gap between columns is about 9 μm, resulting in a porosity of 0.99. After a series of conformal coatings, the gap of the same structure was reduced to 550 nm at the top (figure 8(b)), and less than 50 nm at the bulk of the column array (figure 8(c)), resulting in a porosity of 0.01—a change of two orders of magnitude.

The large variation in the porosity of the structure could be used to span a very wide range of fluid permeability. The flow through an array of cylinders with constant cross-section and uniform pitch was solved by Bruschke [40]. Bruschke showed that for the case of a Newtonian fluid, the lubrication theory predicts that the fluid permeability K_p of a uniform

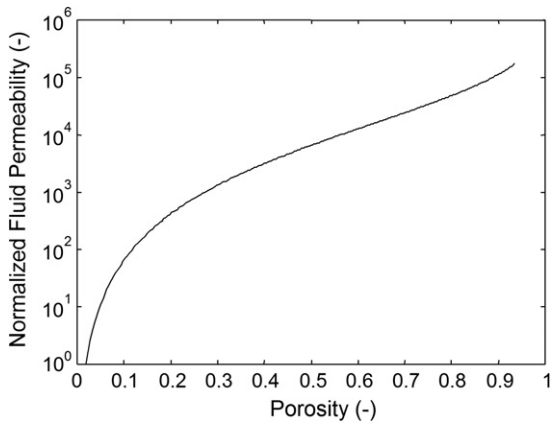

Figure 9. Normalized fluid permeability versus porosity for a column array with hexagonal packing and 10 μm pitch.

array of columns with diameter D and column diameter-to-column pitch ratio Ω is

$$K_p = \frac{D^2}{12}\frac{[1-\Omega^2]^2}{\Omega^3}\left[3\Omega\frac{\tan^{-1}\left[\sqrt{\frac{1+\Omega}{1-\Omega}}\right]}{\sqrt{1-\Omega^2}} + \frac{1}{2}\Omega^2 + 1\right]^{-1}. \quad (1)$$

Based on equation (1), we estimated the normalized fluid permeability (fluid permeability divided by the smallest calculated fluid permeability value) of a hexagonal array of columns (maximum packing density) with 10 μm pitch (figure 9). The result of the analysis suggests that it is possible to vary by more than five orders of magnitude the fluid permeability using the structure that we report. Therefore, the structure can be used as hydraulic impedance for a wide range of flowrates. In particular, this technology would be helpful in implementing multiplexed internally-fed micro/nanofluidics. Researchers have reported some non-uniformities in the performance of microfluidic planar arrays that use an external sintered disk to provide flow control to each fluidic unit [41]. We believe that the use of a highly tuneable hydraulic impedance with low morphological variation that is monolithically fabricated with the rest of the micro/nanofluidic system will improve its operational uniformity while enabling better system integration and further scaling down of the overall system.

4. Estimation of MWNT diameter from electrical characterization

Electrical characterization of the structure was conducted to corroborate the metrology of the MWNTs from the SEMs. A 1 cm^2 array of isolated MWNTs on top of high-aspect-ratio silicon columns was characterized as field emitter using a transparent grid diode structure at a vacuum level better than 10^{-8} Torr (figure 10). Electrons are extracted by the transparent grid and a fraction of which is transmitted through the transparent grid and collected by a suspended external electrode (collector), biased at a voltage higher than the grid. The intent of the external suspended collector is to allow us

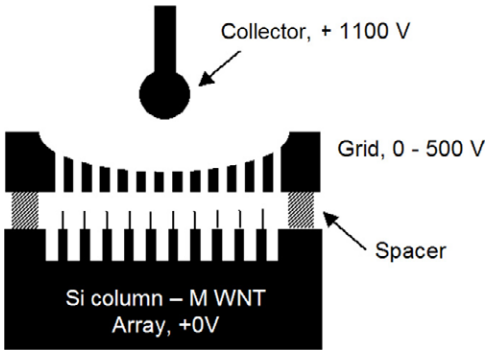

Figure 10. Schematic of transparent grid diode setup. The collector is a 2 mm diameter smooth ball, separated from the grid by about 4 mm. The grid is separated from the substrate by an insulating gasket (spacer) 25 μm thick.

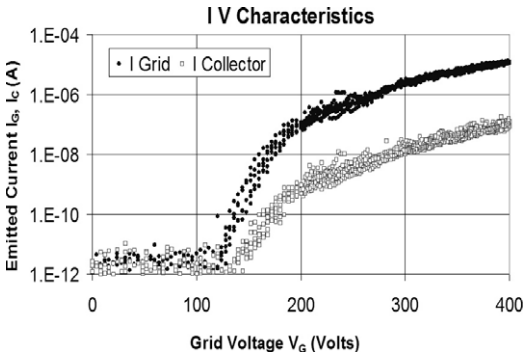

Figure 11. I–V characteristics of the grid and collector currents.

to discriminate between leakage current through the dielectric and electron emission. If the grid and collector currents have a linear dependence, we can conclude that the transparent grid current and the collector have the same physical origin. Since the collector is suspended, then its origin cannot be leakage current through the dielectric.

Figure 11 shows the experimental data of the grid and collector currents from the diode test. From this figure it can readily be seen that the turn-on voltage for electron field emission is about 125 V. Linearity of the grid current and collector current data was verified, resulting in a correlation better than 99.8%. Using the formalism presented by Ding *et al* [42], we defined the turn-on voltage as the voltage at which the emitted current is 1 pA.

Figure 12 is the Fowler Nordheim (FN) plot of the grid current, collector current, and grid plus collector current data from the diode test. In the FN model [43], the electron current I field emitted from a tip biased at a voltage V_G has an exponential dependence with respect to the field factor β:

$$I \propto V_G^2 \exp\left(-\frac{1}{\beta V_G}\right). \tag{2}$$

The inverse of the field factor has dimensions of length. The experimental data in figure 11 can be fitted into straight lines with a correlation better than 99.5%, suggesting that the current is field emitted and described by such model, in agreement with the emission behaviour previously reported by several researchers [32, 33]. The fitted lines in figure 12 have the same slope, further corroborating that the grid current and collector current come from the same source. From the slope of the linear fits of figure 12, a field factor β of 4.79 $\times$ 10^5 cm^{-1} is estimated assuming a workfunction of 4.8 eV. Assuming conservatively that $\beta \sim r^{-1}$ [44], then a MWNT diameter of about 42 nm is calculated from figure 12, in good agreement with the 45 nm value from SEMs (see figure 7(b)). The diameter of a MWNT corresponds to the size of the Ni catalyst sphere that served as template for its growth [21]. Based on the SEM metrology and the I–V characterization, we estimate that each catalyst sphere was formed from an square nanopad 83 nm wide and 7 nm thick. This result

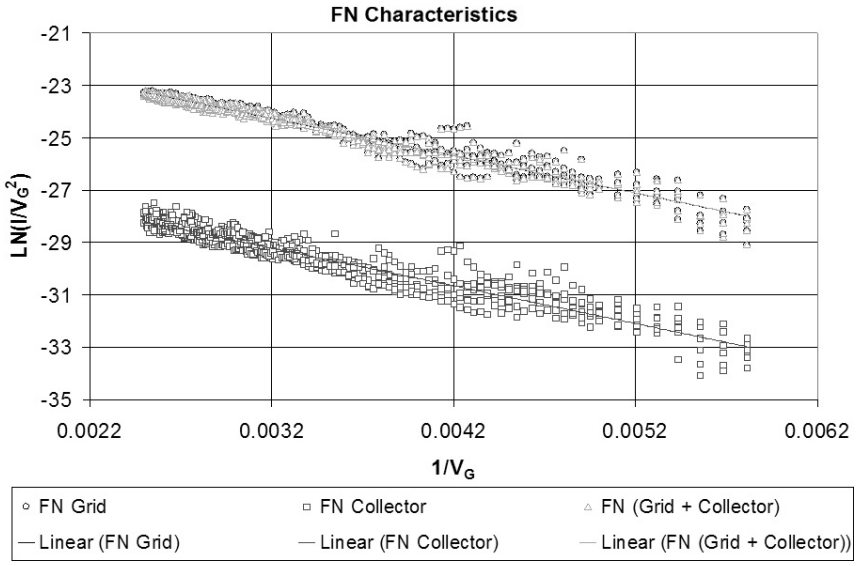

Figure 12. FN plot of grid current, collector current, and grid plus collector currents.

corroborates the reported work of Teo *et al* [21], where they concluded that for Ni, catalyst pads smaller than 300 nm grow only one MWNT. The size of the Ni nanopad is smaller what is achievable by contact photolithography. Therefore, the size of the Ni nanopad was achieved by the wet etching of the Ni film. The proposed fabrication method clearly increases the throughput of isolated CNT growth, compared to electron beam nanolithography.

5. Conclusions

A method for fabricating large arrays of high-aspect-ratio (>100:1), single-crystal silicon columns with submicron tip cross-section is reported. The columns can be either slightly tapered or have a pencil-like morphology and nanoscaled tip diameter. Also, a modification of the method to grow isolated PECVD MWNTs on top of the high-aspect-ratio columns is presented. A process flow to vary the porosity and fluid permeability of the silicon column array over a wide range was documented. Gaps between the vertical pillars were varied between 9 μm and 50 nm. Electron field emission tests on a PECVD MWNT/silicon column array were conducted, and the results are in agreement with the FN model. Based on the FN characterization, the tip diameter of the PECVD MWNT is estimated to be 42 nm, in agreement with the 45 nm value from SEMs. The structure could be used as invasive probe for tissue, as electrical ballast for electron field emitter arrays, and as hydraulic impedance of nanofluidic applications.

Acknowledgments

The authors thank the staff of the MIT's Microsystems Technology Laboratories (MTL) for their help in the fabrication of the structures. The work reported in this paper was sponsored by AFOSR, DARPA/MTO and the US Army Soldier Systems Center (Natick, MA) through contracts No. W911QY-05-1-0002 (DARPA programme manager Dennis Polla, and Army programme manager Henry Girolamo), and FA 9550-06-C-0058 (AFOSR programme manager Major Ryan Umstadt).

References

[1] Ehrfeld W and Schmidt A 1998 *J. Vac. Sci. Technol.* B **16** 3526–34
[2] Wollersheim O *et al* 1994 *J. Micromech. Microeng.* **4** 84–93
[3] Angelo R, Gelorme J, Kuczynski J, Lawrence W, Pappas S and Simpson L 1992 *US Patent Specification* 5.102.772
[4] Bertsh A, Lorenz H and Renaud P 1999 *Sensors Actuators* A **73** 14–23
[5] Boisen A, Hansen O and Bouwstra S 1996 *J. Micromech. Microeng.* **6** 58–62
[6] Hanein Y, Schabmueller C G J, Holman G, Lucke P, Denton D and Bohringer K F 2003 *J. Micromech. Microeng.* **13** S91–5
[7] Robbie K, Brett M J and Lakhtakia A 1996 *Nature* **384** 616
[8] Zhao J P, Ye D X, Wang G C and Lu T M 2002 *Nano Lett.* **2** 351–4
[9] Lehmann V and Foll H 1990 *J. Electrochem. Soc.* **137** 653–9
[10] Lehmann V 1993 *J. Electrochem. Soc.* **140** 2836–43
[11] Laermer F and Schilp A 1994 *US Patent Specification* 5.501.893
[12] Ayon A, Braff R, Bayt R, Sawin H H and Schmidt M A 1999 *J. Electrochem. Soc.* **146** 339
[13] Ayon A, Braff R, Bayt R, Sawin H H and Schmidt M A 1999 *J. Electrochem. Soc.* **146** 2730
[14] Noda S, Tomoda K, Yamammoto N and Chutinan A 2000 *Science* **289** 604–6
[15] Losey M W, Schmidt M A and Jensen K F 2001 *Ind. Eng. Chem. Res.* **40** 2555–62
[16] Günther A, Jhunjhunwala M, Thalmann M, Schmidt M A and Jensen K F 2005 *Langmuir* **21** 1547–55
[17] London A P, Epstein A H and Kerrebrock J L 2001 *J. Propul. Power* **17** 780–7
[18] Frechette L G, Jacobson S A, Breuer K S, Ehrich F F, Ghodssi R, Khanna R, Wong Ch-W, Zhang X, Schmidt M A and Epstein A H 2005 *J. Microelectromech. Syst.* **14** 141–52
[19] Suzuki Y S and Tai Y-C 2006 *J. Microelectromech. Syst.* **15** 1364–70
[20] Carlen E T, Heng K-H, Bakshi S, Pareek A and Mastrangelo C H 2005 *J. Microelectromech. Syst.* **14** 1144–55
[21] Teo K B K *et al* 2003 *Nanotechnology* **14** 204–11
[22] Rosolen G C 1999 *Appl. Surf. Sci.* **144/145** 467–71
[23] Vossen J L and Kern W (ed) 1991 *Thin Film Processes II* (San Diego, CA: Academic)
[24] Schuettler M, Stiess S, King B V and Suaning G J 2005 *J. Neural Eng.* **2** S121–8
[25] Cunningham W *et al* 2001 *J. Phys. D: Appl. Phys.* **34** 2804–9
[26] Mathieson K *et al* 2004 *IEEE Trans. Nucl. Sci.* **51** 2027–31
[27] Velásquez-García L F and Akinwande A I, Microstructures for fluidic ballasting and flow control *US Patent* pending
[28] Tan Y-C, Fisher J S, Lee A I, Cristini V and Lee A P 2004 *Lab Chip* **4** 292–8
[29] Garstecki P, Fischbach M A and Whitesides G M 2005 *Appl. Phys. Lett.* **86** 244108
[30] Tezcan D S *et al* 2007 *Technical Digest IEEE Int. Electron Device Mtg (Washington, DC)* pp 839–42
[31] Byunghoon B, Junghoon Y, Raddadia A D, Masel R I and Shannon M A 2007 *Technical Digest IEEE Solid state Sensors, Actuators and Microsystems Conf. (Lyon)* pp 1497–500
[32] Murakami H, Hirakawa M, Tanaka C and Yamakawa H 2000 *Appl. Phys. Lett.* **76** 1776
[33] Teo K B K *et al* 2002 *Appl. Phys. Lett.* **80** 2011
[34] Velásquez-García L F, Adeoti B, Niu Y and Akinwande A I 2007 *Technical Digest IEEE Int. Electron Device Mtg (Washington, DC)* pp 599–602
[35] Campbell S A 1996 *The Science and Engineering of Microelectronic Fabrication* (New York: Oxford University Press)
[36] Madou M J 2002 *Fundamentals of Microfabrication* 2nd edn (Boca Raton, FL: CRC Press) chapter 2, p 105
[37] Frechete L G *et al* 2000 *Technical Digest IEEE Solid-State Sensor and Actuator Workshop (Hilton Head SC, June 2000)* pp 43–7
[38] Hanein Y *et al* 2003 *J. Micromech. Microeng.* **13** S91–5
[39] Lee H C and Huang R C 1990 *IEEE Electron Device Lett.* **11** 579–81
[40] Bruschke M V and Advani S G 1993 *J. Rheol.* **37** 479–98
[41] Deng W, Klemic J F, Li X, Reed M A and Gomez A 2006 *J. Aerosol Sci.* **37** 696–714
[42] Ding M and Akinwande A I 2002 *IEEE Trans. Electron Devices* **49** 2333–42
[43] Gomer R 1993 *Field Emission and Field Ionization* (New York: AIP)
[44] Pflug D G 1996 Modeling the effects of device scaling on field emitter array performance *MS Thesis* Mass. Inst. Technol. Cambridge, USA